

# Morphology of a stream flowing down an inclined plane. Part 1. Braiding

By K. MERTENS<sup>1</sup>, V. PUTKARADZE<sup>1</sup> AND P. VOROBIEFF<sup>2</sup>

<sup>1</sup>Department of Mathematics and Statistics, The University of New Mexico, Albuquerque, New Mexico 87131, USA

<sup>2</sup>Department of Mechanical Engineering, The University of New Mexico, Albuquerque, New Mexico 87131, USA

(Received September 10, 2005)

A jet of fluid flowing down a partially wetting inclined plane usually meanders. In this paper, we demonstrate that meandering on a smooth plane can be suppressed by maintaining a constant volume flow rate. In the absence of meandering, we experimentally observe the jet developing a *braided* structure with non-monotonic width. This flow pattern is theoretically explained as the result of the interplay between surface tension that tends to narrow the jet down and fluid inertia that drives the jet width to expand. The theory also predicts a bifurcation between the braiding regime and a non-meandering non-braiding flow, which is confirmed by experiment.

---

## 1. Introduction

In this paper, we address the question of surface tension versus boundary interactions in the determination of how fluid flows down inclined planes. The five dimensional parameters of relevance for this problem are the fluid kinematic viscosity  $\nu$ , flow rate  $Q$ , coefficient of surface tension  $\gamma$ , density  $\rho$ , and the component of the acceleration due to gravity in the direction of the flow  $g \sin \alpha$ , where  $\alpha$  is the angle of inclination of the plane (measured from the horizontal). Another relevant quantity is the contact angle between the fluid and the surface. It can be interpreted as a quantitative measure of the wetting properties of the surface, from which the extent of interaction at the solid–fluid boundary can be inferred. This interaction enters our model through the value of contact angle which is taken as an adjustable parameter. Indeed, although the contact angle is known to be a varying and fairly complex quantity (deGennes 1985), here it is assumed to have a constant value for the specific pairing of substrate and fluid used in our experiments.

The simplicity of this approximation notwithstanding, we observe it to lead to results quantitatively and qualitatively consistent with our experiments. These experiments reveal the following. It is possible to suppress both secondary instabilities due to surface effects (i.e. roughness), and the initial meandering instability of the flow (which is attributed to variation in the flow rate  $Q$ ). In the absence of these instabilities, a beautiful stationary *braiding* pattern forms in the downstream flow. Earlier it had been believed that such flows were unattainable, as meandering was thought to dominate every sufficiently slow flow (Nakagawa & Scott 1984). In our experiment, however, we produced a controlled environment where the initial meandering instability can be suppressed, thus facilitating observation of stationary flows and accurate prediction of their properties. Moreover, flows manifesting this braiding pattern can be observed



FIGURE 1. A snapshot of water running down an inclined rock in the Sandia Mountain foothills, New Mexico. Note three isolated narrow streams of water, the width variation most apparent in the central stream.

in nature (figure 1). An example of a natural flow with a highly constant flow rate that can exhibit braiding is a thin stream of water seeping through a narrow, sand-filled crack from a relatively large upstream reservoir and falling on a flat rock.

Note that *braiding* here is not to be confused with river braiding which albeit similar in appearance, is caused by a different physical phenomenon, namely erosion (Ikeda, Parker & Sawai 1981), which is outside the scope of phenomena we consider here.

## 2. Experimental observations

Our experimental apparatus is comprised of a flat acrylic sheet (40 cm by 120 cm) mounted on a horizontal pivot, facilitating changes in the angle of inclination  $\alpha$  between the horizontal and the plane of the sheet. A cylindrical reservoir 1.5 m tall, 12 cm in diameter, is mounted above the sheet. Several nozzles with diameters varying from 0.05 cm to 0.3 cm can be connected to the bottom part of the reservoir via flexible tubing. Due to the size and height of the reservoir, fluctuations in the flow rate from the nozzle are very small. The nozzle is positioned 1 cm above the plane of the acrylic sheet, to suppress possible jet instabilities. The fluid in the reservoir is maintained at a constant level by a peristaltic pump. The pump recirculates the fluid captured in a bottom reservoir mounted below the acrylic sheet. This arrangement can sustain a nearly constant flow rate indefinitely (not taking evaporation losses into consideration). The recirculating fluid is a mixture of water and glycerol with trace amounts of food colouring. Its viscosity  $\nu$  can be varied between 1 and 5 cSt by variation of the water–glycerol ratio. After the recirculating flow is established, it undergoes a period of stabilization, lasting from several minutes to half an hour, which can probably be attributed to the time necessary for disturbances to decay beyond a certain value in the fluid in the upper reservoir. At the end of this period, a stationary non-meandering flow pattern emerges (figure 2). For many values of the flow parameters, this stationary pattern varies in width and height (*braiding*), which can be explained thus.

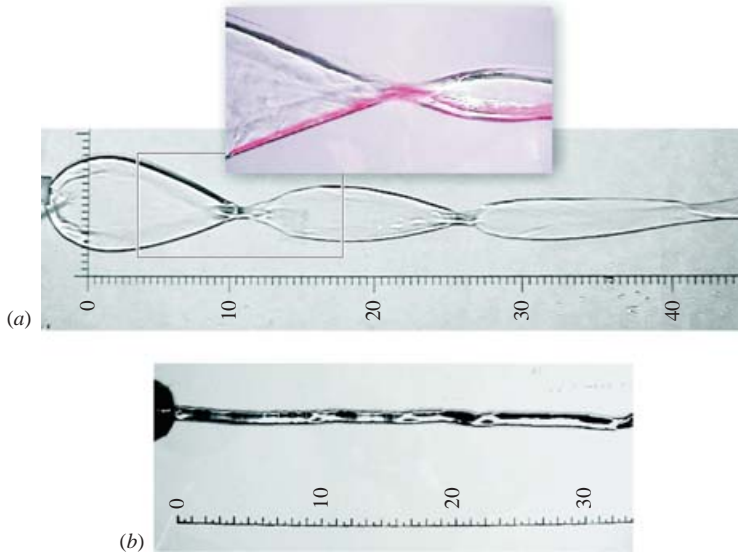


FIGURE 2. Stationary patterns observed in experiment. Flow direction (and the slope of the plane) is from left to right, scale is shown in cm. (a) Braiding pattern. Inset shows injection of red dye demonstrating the *bounce* of the flow near the edge of the stream (see text). Parameter values are: volume flux  $q = 12.2 \text{ cm}^3 \text{ s}^{-1}$ , inclination angle  $\alpha = 45^\circ$ , viscosity  $\nu = 0.016 \text{ cm}^2 \text{ s}^{-1}$ . (b) Non-braiding flow (rivulet) observed with  $q = 2 \text{ cm}^3 \text{ s}^{-1}$ ,  $\alpha = 20^\circ$ ,  $\nu = 0.046 \text{ cm}^2 \text{ s}^{-1}$ .

When the fluid jet discharged from the nozzle strikes the inclined surface, it spreads out due to the inertia of the impact. Most of the fluid is flowing at the outer boundaries of the flow with the interior of the stream being very shallow. Surface tension limits the extent of the spreading and begins to bring the outer boundaries of the flow back together. However, in the process of contraction due to surface tension, the outer edges, carrying most of the fluid, accelerate beyond equilibrium and bounce on impact, as dye injection visualization reveals in figure 2 (a, inset). The boundaries are forced outwards, then collapse again due to surface tension and the process repeats.

This structure is visually reminiscent of the fluid chain structure recently observed by Hasha & Bush (2004) when two fluid jets collide in air at an oblique angle. The amplitude of the subsequent bounces decreases due to viscous dissipation, and far enough downstream the flow assumes a simple profile with a part-circular cross-section, when the surface tension, viscosity and gravity are in balance. The complete solution describing the rivulet of constant width and downstream-distance-independent velocity has only been obtained recently by Perazzo & Gratton (2004).

The issue of the stability of the non-meandering flow pattern will be fully addressed in our next paper on the subject. We conducted some preliminary experiments with acoustic excitation of the flow in the vicinity of the nozzle. The braiding pattern stability is apparently dependent on the volume flux, with more power required to destabilize higher-flux flows. The frequency of the excitation also plays a role. For the flow with volume flux  $q = 11 \text{ cm}^3 \text{ s}^{-1}$  and kinematic viscosity  $\nu = 0.014 \text{ cm}^2 \text{ s}^{-1}$ , a 300 Hz harmonic signal from a 20 W speaker causes the flow to meander, if the speaker diaphragm is 4 cm away from the nozzle. Under the same conditions, a 3000 Hz signal produces no apparent effect. When the excitation is removed, the stationary braided pattern re-establishes itself in the matter of minutes.

### 3. Theory

By using a few basic approximations, and by exploiting some *a priori* knowledge of the system geometry gained from experiment, we can reduce the Navier–Stokes equations governing the system described in the previous section to a coupled set of ordinary differential equations (ODEs). Consider a Cartesian coordinate system with the  $(x, y)$ -plane corresponding to the inclined surface, where the  $(x, z)$ -plane is the plane of symmetry of the flow. Let the width of the stream in the  $y$ -direction be  $w(x)$  and the free surface height in the  $z$ -direction be  $h(x, y)$ . Let us also assume that the  $x$ -component of the velocity  $U_x$  dominates the flow. Previous works (Weiland & Davis 1981; Young & Davis 1987) attempted to describe such flows using long-wavelength approximations, but did not capture the large-amplitude variations observed in experiment.

#### 3.1. Height function

What would be a suitable polynomial approximation for the height function  $h(x, y)$  given our knowledge of the flow morphology? The flow is symmetric with respect to the  $(x, z)$ -plane. In the braided regime,  $h$  can have two local maxima near the edges of the flow when the braids are spread out or one local maximum when they come together. Let us approximate this behaviour by a fourth-order polynomial of the form

$$h(x, y) = (w^2 - y^2)(a - by^2), \quad (3.1)$$

where the  $x$ -dependence is contained in  $w$  and parameters  $a$  and  $b$  are determined by the flow conditions. Parameter  $a$  should be positive to ensure positive  $h(0)$ . To find  $a$  and  $b$ , let us first examine the flow rate  $q$ . If the  $U_x$  velocity component is predominant, let it be independent of  $y$ . Then the flow rate in the  $x$ -direction at any given  $x$  is

$$Q = U_x \int_0^w h(x, y) dy = \text{const}, \quad (3.2)$$

where the integral represents the average area per half-braid and the corresponding flow rate  $Q = q/2$ . This notation uses the symmetry of the flow to simplify the calculations that follow. We will refer to (3.2) as the flux condition.

Second, let us assume that the contact angle  $\theta$  between the free surface and the plane is constant. If the variation in the free surface width and height with  $x$  is moderate, this condition can be approximated as

$$\frac{dh(\pm w)}{dy} = \mp \tan \theta. \quad (3.3)$$

By differentiating (3.1) and combining it with (3.3), we obtain

$$a = \frac{\tan \theta}{2w} + bw^2. \quad (3.4)$$

Now we can find  $b$  by substituting (3.1) and (3.4) into the flux condition (3.2), integrate the latter and solve the result for  $b$ :

$$b = \frac{15}{8w^5} \left( \frac{Q}{U_x} - \frac{\tan \theta w^2}{3} \right). \quad (3.5)$$

The capillary force can be represented as  $f(y) = h'''(y) = 24\gamma by$  for a given  $x$ . With this taken into consideration, we can compute the average capillary force acting on

the half-braid as

$$F = \int_0^w h(y)f(y) dy.$$

Evaluation of this integral produces

$$F = 3b\gamma \tan \theta w^3 + 4\gamma b^2 w^6 = \gamma F_*, \quad (3.6)$$

where  $F_*$  is dimensionless. It is now possible to write the equations of motion.

### 3.2. Equations of motion

Let us begin with the boundary layer approximation in the direction parallel to the plane:

$$\mathbf{U} \cdot \nabla \mathbf{U} = \frac{1}{\rho} \nabla p + g \sin \alpha \hat{e}_x + \nu \frac{\partial^2 \mathbf{U}}{\partial z^2},$$

where  $\hat{e}_x$  is the unit vector in the streamwise direction, and  $\nu$  is kinematic viscosity.  $\mathbf{U}$  and  $\nabla$  in this equation are three-dimensional, but only the  $x, y$  components of the equation are considered. This equation is complemented by the incompressibility condition  $\text{div } \mathbf{U} = 0$ .

Hydrostatic pressure and the contribution of surface tension are combined in pressure  $p$ . In the following analysis we consider only the surface tension contribution, as the role of the hydrostatic term is limited by the shallowness of the flow: a conservative estimate for our experiment shows a 1 : 5 ratio between the hydrostatic and surface tension forces. The viability of this simplification is confirmed by comparison with experiment described in §3.4. Inclusion of the hydrostatic term in the analysis procedure similar to that outlined below would be straightforward, were it necessitated by different flow conditions, e.g. a greatly increased flow rate.

The reduced equations of motion are obtained using integral methods (see Bohr, Putkaradze & Watanabe 1997; Lopez, Miksis & Bankoff 1997; Watanabe, Putkaradze & Bohr 2003). The equations of motion are integrated in the  $y$ -direction from 0 to  $w$  and in the  $z$ -direction from 0 to  $h$ , with the kinematic and dynamic boundary conditions on the free surface taken into account. The total  $y$ -integrated inertial term in direction  $i$  ( $i$  being  $x$  or  $y$ ) is  $(\partial/\partial y)(\rho A U_x U_i)$ , where  $A$  is the area per half-braid. Conservation of flux  $U_x A = Q$  allows us to rewrite the equations of motion as

$$\rho A U_x \left( \frac{\partial}{\partial x} U_y \right) = F - \mu A \frac{1}{h} \frac{\partial U_y}{\partial z} \Big|_{z=0}, \quad (3.7)$$

$$U_x \frac{\partial U_x}{\partial x} = g \sin \alpha - \nu \frac{1}{h} \frac{\partial U_x}{\partial z} \Big|_{z=0}, \quad (3.8)$$

where  $\mu = \nu\rho$  is dynamic viscosity,  $g \sin \alpha$  is the component of acceleration due to gravity in the downstream direction, and  $F$  represents the average capillary force per half-braid (equation (3.6)) as an explicit rational function of  $U_x$  and  $w$ . These partial differential equations including velocity components  $U_x$  and  $U_y$  can be further simplified by making reasonable assumptions about the behaviour of the flow in the  $z$ -direction.

### 3.3. Lubrication approximation

To simplify the velocity derivatives in (3.7), (3.8), let us use the lubrication approximation, assuming that the free surface height  $h(x, y)$  is much smaller than the characteristic scale in the  $x$ -direction. Let us consider a velocity profile in the  $z$ -direction  $U_x(z)$ , such that the velocity is zero at  $z = 0$  (no-slip condition), and there is

no shear on the free surface ( $[dU_x(z)/dz]_{z=h} = 0$ ). Both conditions will be satisfied if a parabolic velocity profile is chosen:

$$U_x(z) = U_s \left( 2\frac{z}{h} - \left(\frac{z}{h}\right)^2 \right).$$

By differentiating, we obtain

$$-\frac{1}{h} \frac{\partial U_x(z)}{\partial z} \Big|_{z=0} = -2 \frac{U_s}{h^2}.$$

We can approximate the constant  $U_s$  in the  $z$ -direction velocity profile by considering  $U_x$  as the average of  $U_x(z)$  with  $z$ -dependence integrated out:

$$\frac{1}{h} \int_0^h U_x(z) dz = U_x.$$

Thus  $U_s = 3/2U_x$  and we can write

$$-\frac{1}{h} \frac{\partial U_x}{\partial z} \Big|_{z=0} = -3 \frac{U_x}{h^2}. \quad (3.9)$$

Now we can also relate  $U_x$  and  $U_y$  using continuity (or mass conservation)

$$U_y = \frac{dw}{dx} U_x.$$

This makes it possible to resolve the second derivative of  $U_y$  as well:

$$-\frac{1}{h} \frac{\partial U_y}{\partial z} \Big|_{z=0} = -\frac{1}{h} \frac{\partial U_x}{\partial z} \Big|_{z=0} \frac{dw}{dx} = -3 \frac{U_x}{h^2} \frac{dw}{dx}. \quad (3.10)$$

### 3.4. Dimensionless equations of motion

By combining the original equations of motion (3.7), (3.8) with our results from the previous subsection (3.9), (3.10), we obtain a system with respect to  $w$  and  $U_x$  and with differentiation in the  $x$ -direction only. By considering  $U_x = U_x(x)$  (flux condition, (3.2)) and replacing  $h$  in (3.9) and (3.10) with  $h_{avg} = A/w = Q/(U_x w)$ , we obtain a system of two coupled ODEs with respect to  $w$  and  $U_x$ .

For further analysis, let us represent this system in dimensionless form. Our problem has five dimensional parameters  $Q$ ,  $g \sin \alpha$ ,  $\rho$ ,  $\nu$ ,  $\gamma$  and one dimensionless parameter  $\theta$ . A group of three dimensionally independent parameters can be constructed. Let us define length and velocity scales  $L$  and  $V$  and dimensionless variables  $x_*$ ,  $w_*$  and  $u_*$  thus:

$$x = Lx_*, \quad w = Lw_*, \quad U_x = Vu_*$$

Then

$$\frac{d}{dx} = \frac{d}{dx_*} \frac{dx_*}{dx} = \frac{1}{L} \frac{d}{dx_*}$$

and the governing equations become

$$\begin{aligned} \frac{d}{dx_*} \left( u_* \frac{dw_*}{dx_*} \right) &= \frac{\gamma L}{Q V \rho} F_* - \frac{3\nu L}{Q} \frac{A}{h^2} \left( u_* \frac{dw_*}{dx_*} \right) \\ u_* \frac{du_*}{dx_*} &= \frac{Lg \sin \alpha}{V^2} - \frac{3\nu L^3 V}{Q^2} u_*^3 w_*^2 \end{aligned}$$

There is one more length scale  $Z$  characterizing the vertical extent of the flow ( $z = Zz_*$ ), although after the  $z$ -dependence is removed by using the lubrication approximation, it only remains implicitly present in the term  $A/h^2$  in the first equation:

$$\frac{A}{h^2} = A \frac{1}{(Zh_*)^2} = \frac{Q}{Vu_*} \frac{1}{(Zh_*)^2} = \frac{Q}{VZ^2} \frac{1}{u_* h_*^2}.$$

By setting the coefficient of  $F_*$  in the first equation and the constant in the second equation to unity, we resolve the length and velocity scale in the  $(x, y)$ -plane:

$$L = \frac{\rho^2 Q^2 g \sin \alpha}{\gamma^2}, \quad V = \frac{\rho Q g \sin \alpha}{\gamma}.$$

Then the dimensionless coefficient of  $A/h^2$  can be also set to unity, yielding for  $Z$

$$Z = \sqrt{\frac{\gamma}{\rho g \sin \alpha}}.$$

Thus  $Z$  is a modified capillary length. With the dimensionless coefficient of  $A/h^2$  thus disposed of, we can rewrite this quantity as  $w_*^2 u_*$  and thus obtain the final form of the system of equations

$$(u_* w'_*)' = F_* - \Pi_{\text{I}} u_*^2 w_*^2 w'_*, \quad (3.11)$$

$$u_* u'_* = 1 - \Pi_{\text{II}} u_*^3 w_*^2, \quad (3.12)$$

where  $(\cdot)' = d(\cdot)/dx_*$ , and the dimensionless constants are

$$\Pi_{\text{I}} = \frac{3\nu L}{Q} = \frac{3\nu \rho^2 Q g \sin \alpha}{\gamma^2}, \quad (3.13)$$

$$\Pi_{\text{II}} = \frac{3\nu L^3 V}{Q^2} = \frac{3\nu \rho^7 Q^5 (g \sin \alpha)^4}{\gamma^7}. \quad (3.14)$$

Finally,

$$F_* = \frac{1}{16} \left[ 15 \frac{\Pi_{\text{I}}}{\Pi_{\text{II}}} \frac{1}{u_* w_*^2} - 5 \tan \theta \right] \left[ 15 \frac{\Pi_{\text{I}}}{\Pi_{\text{II}}} \frac{1}{u_* w_*^2} + \tan \theta \right]. \quad (3.15)$$

Equations (3.11) and (3.12) now represent a coupled pair of ODEs for the downstream velocity  $u_*$  and stream width  $w_*$ . These equations explain the braids as an oscillatory approach to a constant velocity and width far downstream. They demonstrate the interaction between inertia, surface tension, and gravity as that constant width solution is approached. The equations can be described qualitatively as follows. As the fluid accelerates, it is drawn together by surface tension, but in the acceleration process ‘too much’ speed is developed and the outside edges which carry most of the fluid bounce on impact (see figure 2a inset). The fluid is then forced outward until surface tension pull again forces a braid collapse and the process repeats. The system (3.11), (3.12) can be solved numerically. The solution faithfully predicts the length of the braids and the evolution of braid amplitude with downstream distance throughout the parameter range we investigated. The r.m.s. of the difference between predicted and experimentally measured width  $w(x)$  did not exceed 1.5% (figure 3a). It is also noteworthy that the free surface shape  $h$  reconstructed from the solution of (3.11), (3.12) bears a very strong resemblance to the actual free surface observed in experiment (figure 3b, c). It is noteworthy that the contact angle used in the numerical simulations was  $54^\circ$ . Due to the hysteresis of contact angle, the

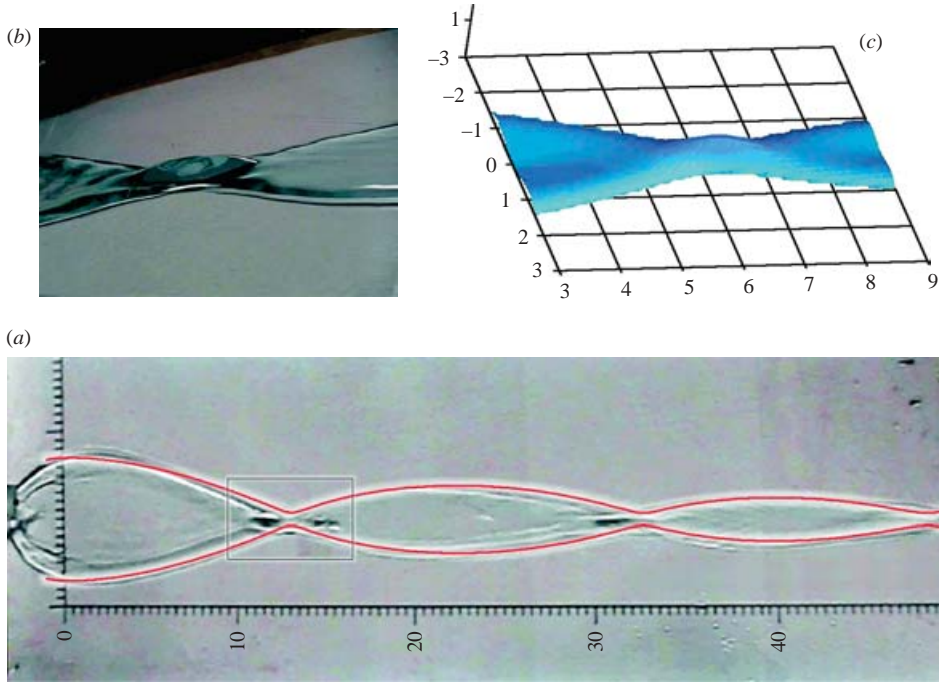


FIGURE 3. Comparison of experiment and theory for braiding with parameter values: volume flux  $q = 12.2 \text{ cm}^3 \text{ s}^{-1}$ , inclination angle  $\alpha = 45^\circ$ , viscosity  $\nu = 0.016 \text{ cm}^2 \text{ s}^{-1}$ . (a) Laboratory experiment (photo) with the prediction of the theoretical model (red line) superimposed. Scale in cm, flow direction is from left to right. (b) Close-up view (at  $30^\circ$  to the plane) of the first braid. (c) Similar view of the first braid according to theory. In, the region corresponding to the close-up is identified by a rectangle.

literature gives a  $50^\circ$ – $60^\circ$  range for contact angles between water–glycerin mixtures and acrylic substrate, hence the contact angle was used as a fitting parameter confined within this range.

### 3.5. Critical points and stability

Further solution analysis may be done to determine critical points, examine linearization around these points, and determine the associated eigenvalue equation for the system (3.11), (3.12). This information may then be used to assess the solution stability and analyse the bifurcation diagram of the system.

By inspection of (3.11), when the force  $F_*$  goes to zero, the system has a critical point, which leads to two possibilities (3.15):

$$\frac{\Pi_I}{\Pi_{II} u_*} = \frac{w_*^2 \tan \theta}{3}, \quad (3.16)$$

$$\frac{\Pi_I}{\Pi_{II} u_*} = -\frac{w_*^2 \tan \theta}{15}. \quad (3.17)$$

It can be shown however that (3.17) leads to instability, thus, from (3.16) and (3.14), for the stable critical point we have

$$u_c = \sqrt{\frac{\tan(\theta)}{3\Pi_{II}}}, \quad w_c = \sqrt{\frac{\tan(\theta)}{\Pi_{II} u_c^3}}. \quad (3.18)$$

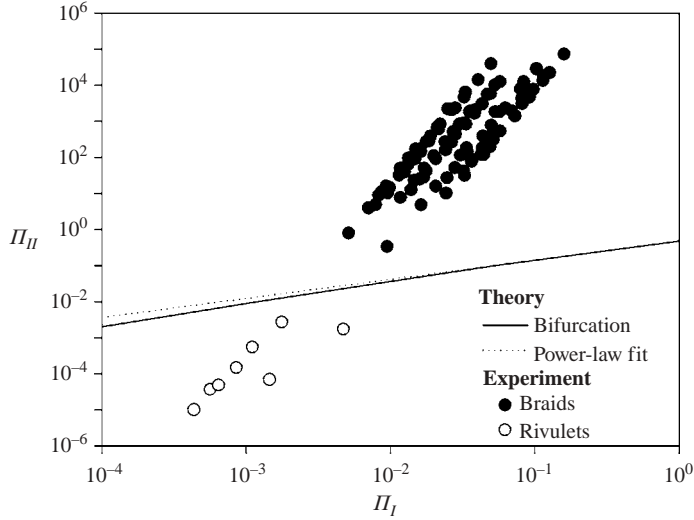


FIGURE 4. Experimental observations of braiding (●) and non-braiding (○) flow in terms of parameters  $\Pi_I$ ,  $\Pi_{II}$ . Solid line: theoretical transition boundary from non-braiding to braiding flow; dotted line: power-law fit (see text).

### 3.6. Linearization and eigenvalue problem

Let us consider linearization near the stable critical point of the previous section

$$u_* = u_c + u_1 \exp(\lambda x), \quad w_* = w_c + w_1 \exp(\lambda x),$$

where  $u_1$  and  $w_1$  are small.

Now, to determine the eigenvalues, let us consider  $F_*$  as set by (3.15), and

$$G_* = 1 - \Pi_{II} u_*^3 w_*^2.$$

In terms of  $F_*$ ,  $G_*$  and their derivatives, the eigenvalue problem can be formulated as

$$\det \begin{bmatrix} \left( u_c \lambda^2 - \frac{\partial F_*}{\partial w_*} + 4\Pi_I u_c^2 w_c^2 \lambda \right) & -\frac{\partial F_*}{\partial u_*} \\ -\frac{\partial G_*}{\partial w_*} & u_c \lambda - \frac{\partial G_*}{\partial u_*} \end{bmatrix} = 0. \quad (3.19)$$

To find the eigenvalues, we need to solve a cubic equation in  $\lambda$ . The real part of  $\lambda$  is negative for all parameter values. A pair of complex conjugate eigenvalues corresponds to a solution with oscillating width, i.e. braiding. After (3.19) is solved numerically, the braid length can be determined as  $2\pi/\text{Im}\lambda$ . When the braid length goes to infinity, i.e.  $\text{Im}\lambda \rightarrow 0$ , the stream approaches the rivulet solution (figure 2b, Davis 1980; Perazzo & Gratton 2004).

### 3.7. Bifurcation

The bifurcation diagram in the  $(\Pi_I, \Pi_{II})$ -plane (figure 4 with solid line showing the transition boundary, also see Mertens, Putkaradze & Vorobieff 2004) characterizes the transition from braiding to rivulet-like flow structure, i.e. transition to infinite braid length as  $\text{Im}\lambda \rightarrow 0$ , in good agreement with experiment. The transition line in the parameter range we investigated could be approximated by a power-law fit of  $\Pi_{II} = 4.07\Pi_I^{1.89}$ .

#### 4. Conclusion

We have created a simple model which nevertheless presents an accurate description of the processes which create fluid braids in a flow down an inclined plane with meandering suppressed by maintaining a constant flow rate. The braiding phenomenon is best described as a battle for dominance in the flow structure between the surface tension of the fluid and the inertia of the peripheral zones of the flow under the influence of gravity. By taking advantage of averaging methods for thin film flows, lubrication approximations, and the idea of a constant contact angle, this model provides a simple method by which the flow can be predicted for a given partially wetting surface–fluid combination.

We see that for smaller angles of inclination the braids become wider and shorter. As viscosity is increased, the dissipative terms begin to dominate and braids eventually disappear. Increased flow rate increases braid length, and so does increased inclination angle, while decreased flow rate will eventually lead to rivulet solutions.

A bifurcation in the parameter space of our model corresponds to the transition between braiding and rivulet flows in experiment. Our model also accurately predicts the braid length, as well as the overall flow morphology.

It is also important to note that earlier assumptions that meandering could not be eliminated in the immediate downstream flow are corrected, and in doing so a new inherent instability (braiding) is described.

#### REFERENCES

- BOHR, T., PUTKARADZE, V. & WATANABE, S. 1997 Averaging theory for the structure of hydraulic jumps and separation in laminar free-surface flows. *Phys. Rev. Lett.* **79**, 1038–1041.
- DAVIS, S. H. 1980 Moving contact lines and rivulet instabilities. Part 1. The static rivulet. *J. Fluid Mech.* **98**, 225–242.
- DEGENNES, P. G. 1985 Wetting – statics and dynamics. *Rev. Mod. Phys.* **57**, 827–863.
- HASHA, A. & BUSH, J. W. M. 2004 On the collision of laminar jets: fluid chains and fishbones. *J. Fluid Mech.* **511**, 285–310.
- IKEDA, S., PARKER, G. & SAWAI, K. 1981 Bend theory of river meanders. Part 1. Linear development. *J. Fluid Mech.* **112**, 363–377.
- LOPEZ, P. G., MIKSI, M. J. & BANKOFF, S. G. 1997 Inertial effects on contact line instability in the coating of a dry inclined plate. *Phys. Fluids* **9**, 2177–2183.
- MERTENS, K. M., PUTKARADZE, V. & VOROBIEFF, P. 2004 Braiding patterns on an inclined plane – The changing boundaries of a stream flowing at a constant rate are explained. *Nature* **430** (6996), 165.
- NAKAGAWA, T. & SCOTT, J. 1984 Stream meanders on a smooth hydrophobic surface. *J. Fluid Mech.* **149**, 89–99.
- PERAZZO, C. A. & GRATTON, J. 2004 Navier–Stokes solutions for parallel flow in rivulets on an inclined plane. *J. Fluid Mech.* **507**, 367–379.
- WATANABE, S., PUTKARADZE, V. & BOHR, T. 2003 Integral methods for shallow free-surface flows with separation. *J. Fluid Mech.* **480**, 233–265.
- WEILAND, R. H. & DAVIS, S. H. 1981 Moving contact lines and rivulet instabilities. Part 2. Long waves on flat rivulets. *J. Fluid Mech.* **107**, 261–280.
- YOUNG, G. W. & DAVIS, S. H. 1987 Rivulet instabilities. *J. Fluid Mech.* **176**, 1–31.